1 **The tolerance to hypoxia is defined by a time-sensitive response of the**

2 **gene regulatory network in sea urchin embryos**

3 **Running title: Regulatory response to hypoxia**

4 Majed Layous, Lama Khalaily, Tsvia Gildor and Smadar Ben-Tabou de-Leon[*]

5 Department of Marine Biology, Leon H. Charney School of Marine Sciences, University of Haifa,

6 Haifa 31905, Israel.

7 *Correspondence: Smadar Ben-Tabou de-Leon (sben-tab@univ.haifa.ac.il)

8

9 Key words:

10 Hypoxia, Gene regulatory networks, Sea urchin, Deoxygenation, Evolution and development,

11 Skeletogenesis

12

13 **Summary statement** (<=30 words)

14 The use of hypoxia and redox gradients as morphogens makes sea urchin early development

15 sensitive to environmental hypoxia. This sensitivity decreases later, due to the structure of the gene

16 regulatory network.

17
18

Abstract (<=180 words)

Deoxygenation, the reduction of oxygen level in the oceans induced by global warming and anthropogenic disturbances, is a major threat to marine life. This change in oxygen level could be especially harmful to marine embryos that utilize endogenous hypoxia and redox gradients as morphogens during normal development. Here we show that the tolerance to hypoxic conditions changes between different developmental stages of the sea urchin embryo, due to the structure of the gene regulatory networks (GRNs). We demonstrate that during normal development, bone morphogenetic protein (BMP) pathway restricts the activity of the vascular endothelial growth factor (VEGF) pathway to two lateral domains and by that controls proper skeletal patterning. Hypoxia applied during early development strongly perturbs the activity of Nodal and BMP pathways that affect VEGF pathway, dorsal-ventral (DV) and skeletogenic patterning. These pathways are largely unaffected by hypoxia applied after DV axis formation. We propose that the use of redox and hypoxia as morphogens makes the sea urchin embryo highly sensitive to environmental hypoxia during early development, but the GRN structure provides higher tolerance to hypoxia at later stages.

Introduction

During the evolution of metazoans, animals were exposed to variations in oxygen levels and molecular mechanisms evolved to enable organisms to cope with hypoxic conditions (Semenza, 2012). However, it is still unclear whether these mechanisms are sufficient to protect marine organisms and specifically, their embryos, from the acute hypoxic conditions that become more common in the oceans (Altieri et al., 2017; Breitburg et al., 2018; Hughes et al., 2020). In the last 50 years the dissolved oxygen (O_2) content of the global ocean has decreased by more than 2%, apparently due to warming that reduces oxygen solubility and increases biological consumption (Schmidtko et al., 2017). Recent studies indicate that oxygen loss in the oceans, termed deoxygenation, is more lethal to marine life than the direct effect of the rising temperatures or ocean acidification (Altieri et al., 2017; Breitburg et al., 2018; Hughes et al., 2020; Schmidtko et al., 2017; Vaquer-Sunyer and Duarte, 2008). The embryos of marine organisms could be highly sensitive to deoxygenation; especially embryos that use endogenous hypoxia and redox gradients as morphogens to guide the activation of gene regulatory networks (GRNs) during normal development (Chang et al., 2017; Coffman and Su, 2019; Cordeiro and Tanaka, 2020; Dunwoodie, 2009; Lendahl et al., 2009). Deciphering the structure and function of developmental GRNs that are activated by hypoxia and redox morphogens is a key to understand this fundamental regulatory mechanism as well as to assess the expected effect of ocean deoxygenation on marine embryos.

The sea urchin embryo provides an attractive system to study the developmental GRNs that are driven by variation in oxygen and redox levels and the effect of hypoxic conditions on these GRNs. Sea urchins are major grazers in shallow seas and coastal waters across the oceans (Pearse, 2006) and adult sea urchins were shown to be moderately sensitive to hypoxic conditions (Hughes et al., 2020; Low and Micheli, 2018; Suh et al., 2014; Vaquer-Sunyer and Duarte, 2008). The experimental advantages of sea urchin embryos and the role of the sea urchins in marine ecology make them a prominent model system for developmental and ecological studies (Pearse, 2006; Peter and Davidson, 2011; Sethi et al., 2012). The models of the gene regulatory networks that drive sea urchin early development are the state of the art in the field (Morgulis et al., 2019; Oliveri et al., 2008; Peter and Davidson, 2011). Importantly, the sea urchin GRNs use endogenous oxygen and redox gradients as developmental morphogens that drive the formation of the dorsal-ventral (DV) axis (Chang et al., 2017; Coffman et al., 2014; Suh et al., 2014).

During early development of the sea urchin embryo, maternally induced oxygen and redox gradients initiate the localized activity of several signaling pathways that eventually control the patterning along the DV axis (Fig. 1, (Chang et al., 2017; Coffman et al., 2014; Suh et al., 2014)).

3

68 In the eggs of the sea urchins, the mitochondria are concentrated at the future ventral side (Coffman
69 et al., 2004; Coffman et al., 2014), which leads to the formation of redox and oxygen gradients in
70 the early embryos (Fig. 1A, (Agca et al., 2009; Coffman et al., 2004)). Specifically, the
71 mitochondria produces reactive oxygen species (ROS) that generate an oxidizing environment
72 which activate redox sensitive transcription factors that activate the expression of the Nodal ligand
73 in the ventral ectoderm (Agca et al., 2009; Coffman et al., 2004; Coffman et al., 2014). Nodal
74 reception drives the expression of the Nodal ligand and its antagonist Lefty and the positive and
75 negative feedback interactions between these two proteins define the boundaries of the ventral
76 ectoderm (Fig. 1B, (Duboc et al., 2008; Duboc et al., 2004)). Nodal activity drives the expression
77 of the Bone Morphogenetic Protein (BMP), BMP2/4, and its antagonist Chordin, forming an
78 incoherent feedforward loop (Fig. 1C, (Agca et al., 2009; Coffman et al., 2004; Coffman et al.,
79 2014)). Chordin prevents the binding of BMP2/4 to its receptor at the ventral side so BMP is
80 received only at the dorsal side where it activates gene expression through the phosphorylation of
81 the transcription factor SMAD1/5/8 (Ben-Tabou de-Leon et al., 2013; Duboc et al., 2004; Lapraz
82 et al., 2009) (Fig. 1C, D). Another early regulator of dorsal gene expression is the transcription
83 factor, hypoxia-inducible factor 1α (HIF1α) that is stabilized in the dorsal side of the sea urchin
84 blastula, apparently downstream of the oxygen gradient (Fig. 1A, B, (Ben-Tabou de-Leon et al.,
85 2013; Chang et al., 2017; Coffman et al., 2009)). Thus, sea urchin embryos use the Nodal and BMP
86 pathways and HIF1α to generate their DV axis downstream of redox and oxygen gradients inherited
87 from the sea urchin egg.

88 Growth in hypoxic conditions leads to radialization of sea urchin embryos with prominent effects
89 on the larval skeleton (Agca et al., 2009; Coffman et al., 2004). The skeleton of the sea urchin
90 larvae is made of two skeletal calcite rods, the spicules, that are formed within a tubular syncytial
91 chord produced by the skeletogenic cells (Morgulis et al., 2019; Oliveri et al., 2008). When the
92 embryos are grown in hypoxic conditions the formation of the DV axis and the skeleton are
93 disrupted, the spicules do not elongate properly and the embryonic morphology is significantly
94 deformed (Agca et al., 2009; Coffman et al., 2004).

95 Sea urchin skeletogenesis depends on the Vascular Endothelial Growth Factor (VEGF) pathway,
96 an essential regulator of vertebrates' vascularization and of tubulogenesis in other phyla (Potente
97 et al., 2011; Tettamanti et al., 2003; Tiozzo et al., 2008; Yoshida et al., 2010). The VEGF Receptor
98 (VEGFR) is expressed in the sea urchin skeletogenic cells together with five transcription factors
99 whose homologs are essential for vertebrates' vascularization (Adomako-Ankomah and Ettensohn,
100 2013; Duloquin et al., 2007; Morgulis et al., 2019; Sun and Ettensohn, 2014). This and other

4

101 similarities between the sea urchin skeletogenic gene regulatory network (GRN) and the

102 vertebrates' vascularization GRN suggest that these GRNs evolved from a common ancestral

103 tubulogenesis GRN (Morgulis et al., 2019). The VEGF ligand is secreted from two lateral

104 ectodermal domains located between the dorsal and the ventral ectoderm (Fig. 1D, (Adomako-

105 Ankomah and Ettensohn, 2013; Duloquin et al., 2007; Morgulis et al., 2019)). VEGF expression

106 is repressed in the ventral ectoderm by the transcription factor Not1 that is activated by Nodal

107 signaling (Fig. 1D, (Li et al., 2012)). Yet, the regulatory links between BMP, HIF1α and VEGF

108 signaling and how VEGF and BMP pathways are affected by hypoxia are not known.

109 Overall, sea urchin DV axis formation and skeletogenesis are strongly affected by hypoxic

110 conditions and are regulated by Nodal, BMP, VEGF and HIF1, downstream of maternal oxygen

111 and redox gradients (Fig. 1). To understand the effect of exogenous hypoxia on sea urchin

112 development, here we study the regulatory links between the sea urchin DV and skeletogenic GRNs

113 during normal development and under hypoxia applied at different developmental stages. We

114 reveal that these two GRNs are strongly connected through the interactions between the BMP and

115 VEGF pathways and that the DV GRN is hypersensitive to hypoxia during early development but

116 becomes relatively tolerant to low oxygen levels with developmental progression.

Results

Sea urchin BMP2/4 controls skeletal patterning and VEGF expression

119 We first wanted to elucidate the links between BMP and VEGF signaling and the effect of BMP

120 signaling on skeletogenic gene expression during normal sea urchin development. To that end, we

121 knocked-down (KD) BMP2/4 expression by the injection of translation morpholino

122 oligonucleotides (MO) into the eggs of the Mediterranean sea urchin species, *Paracentrotus lividus*

123 (*P. lividus*, Fig. 2, see methods for details). Embryos injected with BMP2/4 MO show two major

124 skeletogenic phenotypes: the formation of ectopic spicules in addition to the normal two spicules

125 (ES, Fig. 2B) and ectopic skeletal branching, where the basic structure of two spicules is still

126 observed (EB, Fig. 2C). These observations are in agreement with previous studies of BMP

127 perturbations (Duboc et al., 2004; Lapraz et al., 2009). The expression level of *VEGF* is largely

128 unchanged in BMP morphants (QPCR, Fig. 2G) but its spatial expression expands to one side of

129 the ectoderm (detected by whole mount *in-situ* hybridization [WMISH], Fig. 2D). Since BMP

130 signaling induces dorsal specification (Duboc et al., 2004; Lapraz et al., 2009), *VEGF* expansion

131 in BMP morphants is most likely, to the domain that would normally be specified as dorsal

132 ectoderm. Hence, this data implies that BMP activity represses *VEGF* expression in the dorsal

133 ectoderm in normal embryos.

5

134   To further understand the regulatory links between the ectoderm and the skeletogenic GRNs, we

135   studied the effect of BMP2/4 KD on the spatial expression of *VEGFR* and its target gene, the

136   Spicule-Matrix protein 30 (SM30), at the gastrula stage (Duloquin et al., 2007; Morgulis et al.,

137   2019). In control embryos, the expression of *VEGFR* is localized to the two skeletogenic cell

138   clusters where the spicules first form (Fig. 2E) and the expression of *SM30* is noticeably enhanced

139   in these clusters (Fig. 2F). BMP2/4 KD leads to two distinct expansion patterns of the expression

140   of *VEGFR* and *SM30* (Fig. 2E, F). Some embryos show a continuous expansion of *SM30* and

141   *VEGFR* expression throughout the dorsal skeletogenic cells which could drive the ectopic

142   branching phenotype (EB in Fig. 2E, F). However, in some embryos *VEGFR* and *SM30* are

143   expressed in three or four distinct cell clusters, which could be the cell clusters where ectopic

144   spicules form in BMP2/4 KD (ES in Fig. 2E, F). The levels of *VEGFR* and *SM30* mRNA do not

145   show significant change in BMP2/4 MO at one and two days post fertilization (dpf, Fig. 2G).

146   Overall, the expression of *VEGFR* and *SM30* expands in BMP KD, which could underlie the growth

147   of ectopic spicules and ectopic spicule branches in this condition.

148   The expansion of *VEGFR* and *SM30* expression in BMP morphants is probably due to the

149   combination of direct and indirect regulation of these genes by BMP signaling. *VEGFR* and *SM30*

150   could be directly repressed by the BMP pathway through the phosphorylation of the transcription

151   factor SMAD1/5/8 in the dorsal skeletogenic cells. Phosphorylated SMAD1/5/8 (pSMAD1/5/8) is

152   indeed detected in the dorsal skeletogenic cells at the gastrula stage (Lapraz et al., 2009; Lapraz et

153   al., 2006; Luo and Su, 2012) (Fig. 1D), where it activates the expression of *tbx2/3* and *gatac (Duboc*

154   *et al., 2010)*. The expression of *VEGFR* and *SM30* in BMP morphoants could be also enhanced

155   indirectly, through the expansion of *VEGF* expression in these embryos (Fig. 2D). Together, our

156   results suggest that BMP2/4 signaling controls sea urchin skeletal patterning, through the repression

157   of *VEGF* expression in the dorsal ectoderm, and the repression of *VEGFR* and *SM30* in the dorsal

158   skeletogenic cells.

159   **HIF1α does not regulate skeletal patterning and VEGF expression in the sea urchin embryo**

160   HIF1 is one of the most potent factors in the hypoxia pathway and specifically, it activates *VEGF*

161   expression during hypoxia induced vascularization in vertebrates (Carmeliet, 2005; Pagès and

162   Pouysségur, 2005). Since the sea urchin HIF1α was shown to participate in early DV specification

163   (Ben-Tabou de-Leon et al., 2013; Chang et al., 2017), we wanted to study the effect of the

164   perturbation of this gene on sea urchin *VEGF* expression. In the sea urchin species,

165   *Strongylocentrotus purpuratus* (*S. purpuratus*), HIF1α KD reduced the early expression of the

166   dorsal transcription factors, Tbx2/3 and Dlx, reduced the extension of the dorsal apex and mildly

167 reduced the elongation of the dorsal skeletal rods (Ben-Tabou de-Leon et al., 2013; Chang et al.,

168 2017). To study the effect of HIF1α perturbation on *VEGF* expression we injected HIF1α

169 translation MO into the eggs of the sea urchin, *P. lividus* (Fig. 3). HIF1α KD did not result with

170 distinct skeletogenic phenotypes, in agreement with its weak effect on *S. purpuratus* skeletogenesis

171 (Chang et al., 2017) (Fig. 3A).

172 We tested the effect of HIF1α KD on gene expression level at two developmental time points: 15

173 hours post-fertilization (hpf) which is equivalent to the developmental time where HIF1α activates

174 its dorsal target genes in *S. purpuratus*, and 19hpf, when the effect of HIF1α perturbation starts to

175 decrease in *S. purpuratus* (Ben-Tabou de-Leon et al., 2013). HIF1α KD decreases the expression

176 level of its known target genes, *Pl-tbx2/3* and *Pl-dlx*, with a stronger reduction in the earlier time

177 point, similarly to its effect in *S. purpuratus* (Ben-Tabou de-Leon et al., 2013), supporting the

178 specificity of HIF1α MO (Fig. 3B). However, HIF1α KD does not affect *VEGF*, *VEGFR* and

179 *BMP2/4* expression level at both times. Additionally, HIF1α KD does not affect the spatial

180 expression of *VEGF* in the two time points (Fig. 3C). Thus, our results indicate that the role of

181 HIF1α is restricted to dorsal ectoderm regulation, and does not interfere with skeletal patterning

182 and VEGF regulation in the sea urchin embryo.

Rationale of acute early and late hypoxia treatments

184 We sought to study the effect of transient acute hypoxia on sea urchin skeletogenesis and gene

185 expression under hypoxic conditions that are relevant to oxygen environmental levels. The

186 sensitivity to hypoxia changes significantly between different species and for adult sea urchin the

187 reported sub-lethal threshold for hypoxia is 1.22 mg/L O_2 (Sub-lethal threshold means that the

188 animals survive this stress but their growth, reproduction and physiology are damaged (Vaquer-

189 Sunyer and Duarte, 2008)). Water-quality surveys on sites where a massive mortality event

190 occurred, detected levels of 0.5mg/L O_2 and below in the seabed in depth of 10 meters and under

191 (Altieri et al., 2017). We therefore studied the effect of growth in 0.4-0.5 mg/L O_2, which is severe

192 hypoxic conditions, at 18°C, that is the typical temperature for the upper water column in the

193 Mediterranean sea (Mavropoulou A.M, 2020).

194 We specifically wanted to distinguish between the effect of hypoxia applied during the formation

195 of the DV axis and hypoxia applied after the DV axis is established (Duboc et al., 2004; Lapraz et

196 al., 2009; Nam et al., 2007; Range et al., 2007). Starting at the early blastula, the expression of

197 Nodal, is maintained by an auto-regulation, where Nodal signaling activates the expression of the

198 *nodal* gene (Duboc et al., 2004; Lapraz et al., 2009; Nam et al., 2007; Range et al., 2007). This

199 could indicate that this later phase of development is less sensitive to exogenous hypoxia (Fig. 1B).

7

200   Early blastula occurs in *P. lividus* embryos under normal conditions at about 10hpf (Duboc et al.,

201   2004; Lapraz et al., 2009), but when the embryos are grown in hypoxic conditions their

202   development is slower and they reach this stage at 16hpf. We therefore studied the effect of growth

203   in hypoxic conditions (0.4-0.5 mg/L O_2) for 16 hours, from fertilization and on (early hypoxia,

204   Figs. 4-5), and from early blastula stage and on (late hypoxia, Fig. 6). We observed significant

205   differences in the skeletogenic phenotypes and in gene expression between these two treatments

206   (see methods for the exact protocol).

Early hypoxia distorts skeletal patterning and expands ventral and skeletal gene expression

208   Embryos grown for 16hpf in hypoxic conditions applied immediately from fertilization and on

209   (early hypoxia), are viable and develop into a normally looking blastula, but show severe DV axis

210   disruption and skeletogenic defects from the gastrula stage and on (Fig. 4A-G). This is in agreement

211   with previous works on *S. purpuratus* and indicates that the effect of hypoxic conditions is not

212   species specific (Agca et al., 2009; Chang et al., 2017; Coffman et al., 2009; Coffman et al., 2004;

213   Coffman et al., 2014). At gastrula stage, most of the embryos grown in early hypoxia show irregular

214   skeleton with several ectopic spicules (61%, Fig. 4B, C, G). At pluteus stage, the embryos show

215   partial recovery and display two major skeletogenic phenotypes: A strong phenotype where the

216   skeleton is radialized, the DV axis is disrupted and multiple ectopic spicules are observed (24%,

217   Fig. 4F, G) and a weaker phenotype where the DV axis seems normal but the skeleton shows

218   ectopic spicule branching (41%, Fig. 4E, G). The rest of the embryos developed normally. The

219   skeletogenic phenotypes indicate that hypoxic conditions can strongly affect skeletal patterning

220   probably through changes in skeletogenic gene expression.

221   Next, we investigated the effect of hypoxia on the expression of the DV patterning genes, *nodal*,

222   *BMP2/4* and *chordin*, at blastula and gastrula stages in *P. lividus*. Growth in hypoxic conditions

223   significantly expands *nodal* spatial expression throughout the ectoderm at blastula stage, compared

224   to the ventral localized expression of this gene in normal development (Fig. 4H), in agreement with

225   previous studies in *S. purpuratus* (Coffman et al., 2014). The spatial expression of *BMP2/4* and

226   *chordin* show similar expansion at this time, as expected from downstream target genes of Nodal

227   signaling (Fig. 4I, J). At early gastrula stage, the expression of *nodal* and *BMP2/4* is expanded in

228   embryos grown in hypoxic conditions compared to the expression of these genes in embryos grown

229   in normoxic conditions (Fig. 4K, L). However, the expansion at gastrula stage is not throughout

230   the ectoderm like in the blastula stage, but seems more localized to about a half of the ectoderm, in

231   agreement with the partial phenotypic recovery at the pluteus stage (Fig. 4G).

232   These results suggest that hypoxia leads to the expansion of the ventral ectoderm and probably to

233   the decrease in the dorsal ectoderm domain, which may affect the expression of key skeletogenic

234   regulators, such as *VEGF* and *VEGFR*. Indeed, growth in hypoxic conditions shifts and expands

235   the spatial expression of *VEGF* to one side of the ectoderm, which is most likely the dorsal ectoderm

236   (Fig. 4M). In addition, the expression of *VEGFR* expands beyond the two lateral skeletogenic cell

237   clusters in which it is normally localized (Fig. 4N). Furthermore, the *VEGFR* expressing cells

238   demonstrate the perturbed migration of the skeletogenic cells in hypoxic embryos. This phenotype

239   could be due to the expanded expression of the VEGF ligand that directs the migration of the

240   skeletogenic cells in normal embryos. In sum, growth in hypoxic conditions perturbs the spatial

241   organization of the skeletogenic cells and expands the ectodermal expression of *Nodal, BMP2/4*,

242   *chordin* and *VEGF* and the skeletogenic expression of *VEGFR*.

243   Early hypoxia reduces BMP activity which explains *VEGF* and *VEGFR* expansion

244   The expansion of the ventral side in hypoxic conditions suggests that BMP activity at the dorsal

245   side might be reduced, and the reduction of the repressing BMP activity could explain *VEGF* and

246   *VEGFR* expansion to the dorsal side. To test this hypothesis and monitor BMP activity in normal

247   vs. hypoxic conditions, we performed immunostaining against pSMAD1/5/8. We studied

248   pSMAD1/5/8 signal at two different developmental stages; mesenchyme blastula, when BMP

249   activity is localized at the dorsal ectoderm (Fig. 5A), and at late gastrula, when BMP activity is

250   localized at the dorsal skeletogenic cells (Fig. 5C). Hypoxic conditions completely abolish

251   pSMAD1/5/8 signal from the nuclei of the dorsal ectodermal cells at mesenchyme blastula stage

252   (Fig. 5B). At late gastrula stage, hypoxic conditions eliminate the pSMAD1/5/8 signal from the

253   dorsal skeletogenic cells (Fig. 5D), or strongly reduce it (Fig. 5E). These results indicate, that

254   despite *BMP2/4* expansion in hypoxic embryos, its activity is reduced during hypoxia. The reduced

255   activity can be explained by the expansion of BMP antagonist, Chordin, during hypoxic conditions

256   (Fig. 5C). Together, these results show that BMP activity in the dorsal ectoderm and in the dorsal

257   skeletogenic cells is reduced in hypoxic conditions. Apparently, the reduction of BMP activity

258   removes the repression of *VEGF* and *VEGFR* at the dorsal embryonic domains, leads to their

259   expansion to this domain and to the disruption of skeletal patterning.

260   Late hypoxia mildly affects skeletogenesis and doesn't affect DV and skeletal regulatory genes

261   Our studies show that early hypoxia strongly affects the spatial activity of the main regulators of

262   DV axis formation, Nodal and BMP2/4, and the perturbation of these factors affects skeletal

263   patterning and *VEGF*, *VEGFR* and SM30 expression. Next, we wanted to test whether hypoxia

264   affects skeletogenesis after the DV axis is formed and to investigate the effect of late hypoxic

265 conditions on regulatory gene expression. Thus, we studied the skeletogenic phenotypes of hypoxia

266 applied between 10hpf and 26hpf, which is after the DV axis is established, as explained above.

267 Embryos grown in late hypoxia showed a delayed development and at 26hpf were equivalent to

268 early gastrula stage in normoxic embryos (Fig. 6A, B). At late gastrula and pluteus stages, almost

269 all the embryos grown in late hypoxia show normal skeletal patterning with the two spicules

270 correctly positioned at the two lateral sides (Fig. 6C-G). More than half of the embryos grown in

271 late hypoxia developed ectopic skeletal branching in these two stages, and at pluteus stage, about

272 2% of the embryos show radialized skeleton with ectopic spicules. Overall, late hypoxia induces

273 skeletal defects, such as ectopic branching, but it hardly affects skeletal patterning.

274 We next studied the effect of late hypoxic conditions on the expression of the key regulatory genes

275 investigated above. Late hypoxia treatment does not affect the spatial expression of *nodal* (Fig.

276 6H), in agreement with the normal formation of the DV axis and normal skeletal patterning in this

277 condition. Furthermore, late hypoxia does not affect the spatial expression pattern of *BMP2/4*,

278 *VEGF* and *VEGFR* genes, so these genes are probably not the mediators of the observed mild

279 skeletal defects (Fig. 6I-K). Thus, after the DV axis forms, the expression of the upstream

280 patterning and skeletogenesis regulators, *nodal*, *BMP2/4*, *VEGF* and *VEGFR* is not affected by

281 hypoxic conditions and the skeletal patterning is overall normal.

Discussion

283 GRNs are the genomically encoded programs that control embryonic development, but the

284 environmental conditions in which these GRNs operate can significantly affect their outcome

285 (Beldade et al., 2011; Smith et al., 2018). Particularly, the use of hypoxia and redox gradients to

286 control developmental processes in various phyla, might make the embryos more sensitive to low

287 oxygen levels that are becoming more common in the ocean (Compernolle et al., 2003; Cordeiro

288 and Tanaka, 2020; Dunwoodie, 2009; Semenza, 2012). The structure of the developmental GRN

289 defines its function during environmental hypoxia and underlies the response and resilience to

290 hypoxia during embryogenesis. Here we studied the regulatory linkages and response to transient

291 acute hypoxia of the GRNs that control DV patterning and skeletogenesis in the sea urchin embryo

292 (Fig. 7A, B). We discovered that hypoxia applied during the time where a redox gradient guides

293 the DV axis formation results with a major disruption of the spatial expression of key regulatory

294 genes which explains the radial skeleton formation in these embryos. However, once the DV axis

295 is established, these regulatory genes are no longer affected by hypoxic conditions and skeletal

296 patterning is largely normal. While this suggests that embryos could overcome transient hypoxia if

297 it occurs after their DV axis is formed, hypoxic conditions in natural habitats can last for days and

298 weeks, which is much more than the embryos can tolerate (Altieri et al., 2017). Below we discuss

299 our main findings and their possible implications.

300 Our findings illuminate the regulatory interactions between the DV and skeletogenic GRNs that

301 underlie skeletal patterning in the sea urchin embryo. Previous studies had shown that *VEGF*

302 expression is restricted from the ventral ectoderm by Nodal's target, Not1 (Li et al., 2012), but the

303 mechanism that excludes *VEGF* expression from the dorsal ectoderm was not known. Here we

304 show that BMP activity excludes both *VEGF* from the dorsal ectoderm and *VEGFR* and *SM30* from

305 the dorsal skeletogenic cells, and this exclusion is necessary for spicule initiation to occur only in

306 the ventro-lateral skeletogenic clusters (Fig. 2). We also show that HIF1α, a key activator of VEGF

307 in vertebrates' vascularization (Dunwoodie, 2009; Pagès and Pouysségur, 2005) does not regulate

308 VEGF signaling during early sea urchin development (Fig. 3, 7A). Apparently, the regulatory

309 function of this factor in normal sea urchin development is limited to shaping *nodal* expression

310 domain in the early blastula (Chang et al., 2017), and to activating early dorsal gene expression

311 (Ben-Tabou de-Leon et al., 2013). Thus, BMP signaling restricts VEGF activity to the ventro-

312 lateral skeletogenic clusters and this restriction is required for the exclusion of spicule formation

313 from the dorsal skeletogenic cells in normal sea urchin embryos (Fig. 7A).

314 Early hypoxia in sea urchin embryos strongly distorts the spatial expression of DV and skeletogenic

315 patterning genes, which leads to the formation of ectopic spicules and embryo radialization (Fig.

316 4, 7B). Previous studies have shown that hypoxic embryos are ventralized (Agca et al., 2009) and

317 that *nodal* expression expands in hypoxic conditions (Coffman et al., 2014). Here we revealed the

318 cascade of regulatory interactions that underlie embryo ventralization and the formation of ectopic

319 spicules. Early hypoxia leads to the expansion of *nodal* to the dorsal side, which leads to the

320 expansion of its targets, *BMP2/4* and *chordin* in this condition (Fig. 4H-L, Fig. 7B). The activity

321 of BMP signaling is significantly reduced in both the dorsal ectoderm and dorsal skeletogenic cells

322 as evident from pSMAD1/5/8 staining (Fig. 5). This reduction is probably due to the expansion of

323 the expression of BMP antagonist, *chordin*, into the dorsal side, which blocks BMP activity in early

324 hypoxia embryos (Fig. 4J, 7B). These changes in the spatial activity of Nodal and BMP signaling

325 drive the shift and expansion of *VEGF* and *VEGFR* expression to the dorsal ectoderm and dorsal

326 skeletogenic cells, respectively (Fig. 4M, N 7B). The expansion of VEGF activity to the dorsal

327 skeletogenic cells explains the formation of ectopic spicules in the dorsal side in early hypoxic

328 condition (Fig. 7B). Hence, early hypoxia expands *nodal* expression which reduces BMP activity

329 and specifically, removes the dorsal repression of VEGF signaling, which leads to the formation of

330 ectopic spicules in the dorsal side.

11

331   In striking difference to the strong effect of early hypoxia on the expression of DV and skeletogenic

332   regulatory genes, hypoxia applied after the DV axis is establish does not affect the expression of

333   these genes and results with overall normal skeletogenic patterning (Fig. 6). This resilience of the

334   DV GRN to late hypoxia can be explained by the structure of the GRN, that includes positive and

335   negative feedback loops that restrain Nodal activity (Fig. 7A,B, (Duboc et al., 2008; Nam et al.,

336   2007; Range et al., 2007)). At the early blastula stage, *nodal* expression is maintained by the Nodal

337   pathway through the transcription factor SMAD2/3 (Nam et al., 2007; Range et al., 2007), and

338   *nodal* spatial expression is restricted by its antagonist, Lefty, that is also activated by the Nodal

339   pathway (Fig. 7A, (Duboc et al., 2008)). Once the spatial domain of Nodal activity is established

340   and stabilized by the Nodal-Lefty feedback loops, it is not disrupted by hypoxic conditions,

341   indicating that the redox state is no longer a factor in *nodal* regulation at this stage (Fig. 6H). Nodal

342   spatial activity defines the domain of BMP activity through the Nodal-BMP2/4-Chordin incoherent

343   feedforward loop, which restricts VEGF activity that leads to normal skeletogenic patterning, in

344   late hypoxia embryos (Figs. 6, 7A). This structure of the DV GRN could also underlie the relative

345   restriction of *nodal* expression at the gastrula stage compared to its broad expression at the blastula

346   stage (Fig. 4H, K) and the partial recovery of skeletal patterning in the pluteus stage in early

347   hypoxia (Fig. 4G). Overall, the structure of the DV GRN enables it to partially recover the effect

348   of early hypoxia at later developmental stages and makes it resilient to hypoxia applied after the

349   DV axis had formed.

350   While the effect of the hypoxic conditions on the regulatory cascade downstream of Nodal

351   signaling is quite clear from our findings, the cause of nodal expansion in early hypoxia requires

352   further investigation. Early hypoxia was shown to expand the expression of the HIF1α protein that

353   is normally localized at the dorsal side (Chang et al., 2017). HIF1α transiently represses early *nodal*

354   expression (Chang et al., 2017), yet, HIF1α expansion does not restrict *nodal* expression that

355   expands dorsally in early hypoxia (Fig. 4). Hypoxia was shown to increase ROS levels in cancer

356   cells, smooth muscle cells and endothelial cells, apparently due to its effect on the mitochondria

357   electron transport chain (Chi et al., 2010; Desireddi et al., 2010; Fuhrmann and Brune, 2017;

358   Medini et al., 2020; Tafani et al., 2016). If hypoxia affects the mitochondria in the sea urchin

359   embryo and further increases the ROS levels at the already oxidizing side (Fig. 1), this could

360   underlie the expansion of *nodal* expression in early hypoxia. Thus, *nodal* expansion could be the

361   result of the change in the redox state in hypoxic conditions and the effect of this change on the

362   redox sensitive transcription factors that control *nodal* expression (Agca et al., 2009; Coffman et

363   al., 2004; Coffman et al., 2014; Range et al., 2007). Future research will hopefully illuminate this

364   intriguing regulatory mechanism.

365   Our findings illuminate some similarities between the GRNs that pattern the DV axis and
366   skeletogenesis in the sea urchin embryo and the upstream regulation of vertebrate's vascularization
367   (Lee et al., 2009; Ushio-Fukai and Nakamura, 2008). Hypoxia and redox gradients that regulate
368   DV axis formation and skeletal patterning in the sea urchin embryo, were shown to induce
369   angiogenesis in vertebrates during normal development and in cancer (Chi et al., 2010; Potente et
370   al., 2011). The regulatory interactions between BMP and VEGF that are essential for sea urchin
371   skeletal patterning, also control vertebrates' vascularization, however, they are rather complex:
372   BMP activates VEGF and induces vascularization in some tissues, while it represses VEGF in other
373   tissues (Bai et al., 2013; Dyer et al., 2014; Garcia de Vinuesa et al., 2016; He and Chen, 2005;
374   Wiley et al., 2011). The Nodal pathway does not participate in hypoxia induced vascularization
375   during normal development in vertebrates, however, in various cancer cells, hypoxia drives Nodal
376   expression, which then promotes *VEGF* expression and angiogenesis (Fig. 7C, (Hueng et al., 2011;
377   Quail et al., 2011; Quail et al., 2012)). The transcription factor HIF1α is a key activator of VEGF
378   expression and angiogenesis in vertebrates, but the sea urchin HIF1α does not regulate VEGF
379   signaling during normal development. Sea urchin HIF1α activity is limited to the transient
380   inhibition of *nodal* and the early activation of dorsal genes (Fig. 3, 7) (Ben-Tabou de-Leon et al.,
381   2013; Chang et al., 2017). Overall, regulatory interactions between Nodal, BMP, HIF1 and VEGF
382   pathways and their modulation by hypoxic conditions are observed both during DV and skeletal
383   patterning in the sea urchin embryo and in vertebrates' vascularization, but there are some apparent
384   differences in the linkages. The participation of these common pathways together with the
385   similarity between the skeletogenic and the vascularization GRNs (Morgulis et al., 2019; Oliveri
386   et al., 2008) might indicate that these upstream patterning programs diverged from a common
387   ancestral GRN; yet we cannot exclude convergent evolution at this stage.

388   Our findings have implications on the effect of ocean deoxygenation on embryos that use hypoxia
389   and redox signaling in their development, yet, the major differences between lab experiments and
390   field conditions should be considered. Our analyses and previous studies suggest that the use of
391   hypoxia and redox gradients makes the sea urchin GRNs highly sensitive to acute hypoxia applied
392   in its early developmental stages, but the GRNs are less sensitive to hypoxia applied after the
393   establishment of the DV axis. Yet, hypoxia events in the ocean and in the coastal zones can last for
394   weeks and their lethal effect is observed for months after (Altieri et al., 2017; Hughes et al., 2020).
395   So even if the sea urchin embryos can survive 16 hours of hypoxia, they will probably die in longer
396   periods of low oxygen. Furthermore, in other organisms ROS and hypoxia signaling regulate
397   multiple developmental processes and in some cases, these processes last throughout

398   embryogenesis, which could make the embryos of these organisms even more sensitive to hypoxia

399   than sea urchin embryos (Breus and Dickmeis, 2020; Coffman and Su, 2019; Cordeiro and Tanaka,

400   2020). Within these alarming notions, lab experiments can show distinct and even opposing trends

401   then experiments that are done in the field due to the increased and unexpected complexity of

402   natural sites (Foo et al., 2020). Therefore, further hypoxia studies guided by environmental changes

403   should be done in the field, to elucidate the sensitivity and resilience of the molecular response to

404   hypoxia in marine embryos in their natural habitat.

Materials and Methods

Animals and embryo cultures

407   Adult *P. lividus* sea urchins were purchased from the Institute of Oceanographic and Limnological

408   Research (IOLR) in Eilat, Israel. Eggs and sperm were obtained by injection 0.5M KCl solution to

409   adult sea urchins. Embryos were cultured in artificial seawater (ASW) at 18°C.

Microinjection, RNA extraction and Reverse-transcription

411   The design and preparation of novel morpholino (MO) was done in genetools (http://www.gene-

412   tools.com). Translation of *HIF1α* was blocked by the microinjection of 400-700µM *HIF1α*-MO

413   into sea urchin eggs. *HIF1α*-MO sequence: 5`-GGTCGCCATAATCAGTCTCTGTTTC-3`.

414   Translation of *BMP2/4* was blocked by the microinjection of 400-600µM. *BMP2/4*-MO sequence:

415   5`-GACCCAGTTTGAGGTGGTAACCAT-3`, this MO has been characterized in previous studies

416   (Duboc et al., 2004). The control MO is Random commercial MO which does not have any effect

417   on embryo development, along with 1µg/ml rhodamine dextran (D3329 Molecular probes, OR,

418   USA) and 0.12M KCl. Total RNA was extracted from injected sea urchin embryos (≥120 injected

419   embryos) using RNeasy Micro Kit (50) from QIAGEN (#74004) according to the kit protocol using

420   DNase treatment from RNease-Free DNase Set- Qiagen (50) (#79254). Elution was done in 16.5µl

421   nuclease-free ultra-pure water. Extracted RNAs were then reverse transcribed into cDNA by using

422   SuperScript™ II Reverse Transcriptase (Thermo Fisher scientific 18064022) (10 min 25°C, 2hr in

423   25°C, 85°C for 5 min).

Quantitative-PCR (qPCR) analysis

425   qPCR was performed using the CFX384 Touch™ Real-Time PCR Detection System #1855485.

426   Reactions were carried out in 10µl volume including: 5µl SYBR BioRad IQ SYBR Green Supermix

427   (#1725125), 2.5µl of 1.2µM forward and reverse gene specific primers and 2.5µl of cDNA (qPCR

428   primers used in this study are listed in Table S1). Each cDNA sample was run in triplicate, for

429   every candidate gene, ubiquitin was used as internal control. The reactions thermal profile was:

14

430   95°C for 3 minutes followed by 40 amplification cycles of 95°C for 10 seconds and 55°C for 30

431   sec. Dissociation analysis was performed at the end of each reaction to confirm the amplification

432   specificity. Primer sets for all tested genes were designed using Primer3Plus

433   (http://www.bioinformatics.nl/ cgi-bin/primer3plus/primer3plus.cgi/). Results are presented as the

434   means and standard error of at least two biological replicates. The comparison to an internal

435   standard (ubiquitin) was done in order to determine the expression level of the gene, and the change

436   in the expression levels were measured in comparison to the expression level of the gene in control

437   MO.

Hypoxia treatment

439   ASW were treated with 99.5% Nitrogen (N_2) and 0.5% Oxygen (O_2) to decrease the oxygen

440   solubility in ASW till the dissolved O_2 level was 0.4-0.5 mg/L, creating hypoxic ASW. Embryos

441   were transferred into petri-dish that contains the hypoxic ASW, then the dishes were incubated in

442   a hypoxia chamber at 18°C. The hypoxia chamber is a sealed box that receives a constant flow of

443   99.5% N_2 and 0.5% O_2. To distinguish between the direct effect that hypoxic conditions might have

444   on skeletogenesis and its effect on DV patterning, we studied the skeletogenic phenotypes of

445   hypoxia applied immediately after fertilization (early hypoxic condition) and the effect of hypoxia

446   applied after the DV axis was established (late hypoxic condition). In early hypoxia treatment, the

447   eggs were fertilized, their fertilization envelope was immediately removed and the zygotes were

448   incubated in the hypoxia chamber for 16 hours. In late hypoxia treatment, the eggs were fertilized

449   and the embryos were cultured under normoxic conditions for 10 hours until the blastula stage.

450   Then, the embryos were transferred into the hypoxia chamber and incubated in hypoxic conditions

451   for 16 hours. After 16 hours in hypoxic conditions the embryos were removed from the hypoxia

452   chamber and cultured in normoxic conditions until the pluteus stage.

Probe design and WMISH procedure

454   WMISH probe preparation and WMISH procedure were performed as described in (Morgulis et

455   al., 2019). Primer list is provided in table S2.

Removal of fertilization envelope

457   To perform WMISH on sea urchin embryos at early blastula stage, the fertilization envelope were

458   removed; Fertilized eggs were incubated in presence of Paraminobenzoic acid (PABA, A6928,

459   Sigma) and Amino triazole (ATA, A8056 Sigma) (2mM each at final concentration) to soften the

460   fertilization envelope (FE). After microscopy visualization of FE, FE were removed by flow the

461   zygotes through a 75µm mesh four times. Next, the embryos were washed three times with ASW

462   and grown till the indicated collection time points.

Immunostaining

464   Immunostaining of pSMAD1/5/8 antibody was done similarly to (Lapraz et al., 2009) with minor

465   modifications. Embryos were fixed in 4% paraformaldehyde, 33mM Maleic acid buffer pH7,

466   166mM NaCl, for 10 minutes at room temperature, then embryos exposed to Methanol for 1

467   minute. Embryos were washed four times with PBST, then incubation for 1 hour in blocking

468   solution (PBST and 4% sheep serum), followed by incubation with primary Antibody against

469   pSMAD1/5/8 (the antibody was purchased from Cell Signaling Technology; no. 9511) at 1:200

470   dilution in blocking solution, overnight at 4˚C. Embryos were then washed four time in PBST, then

471   the secondary Antibody was added to the embryos (Peroxidase-conjugated AffiniPure Goat Anti-

472   Rabbit IgG; no. 111-035-003) diluted 1:200 in blocking solution and incubated for 1 hour in room

473   temperature, followed by four washes with PBST. Store solution (PBST in 50% glycerol) at 4˚C.

Imaging

475   All images presented in this study were generated on a Zeiss Axio Imager M2.

Acknowledgments

482

References

484   Adomako-Ankomah, A., Ettensohn, C.A., 2013. Growth factor-mediated mesodermal
485   cell guidance and skeletogenesis during sea urchin gastrulation. Development 140, 4214-
486   4225.
487   Agca, C., Klein, W.H., Venuti, J.M., 2009. Reduced O2 and elevated ROS in sea urchin
488   embryos leads to defects in ectoderm differentiation. Dev Dyn 238, 1777-1787.
489   Altieri, A.H., Harrison, S.B., Seemann, J., Collin, R., Diaz, R.J., Knowlton, N., 2017.
490   Tropical dead zones and mass mortalities on coral reefs. Proc Natl Acad Sci U S A 114,
491   3660-3665.
492   Bai, Y., Wang, J., Morikawa, Y., Bonilla-Claudio, M., Klysik, E., Martin, J.F., 2013.
493   Bmp signaling represses Vegfa to promote outflow tract cushion development.
494   Development 140, 3395-3402.

495 Beldade, P., Mateus, A.R.A., Keller, R.A., 2011. Evolution and molecular mechanisms of
496 adaptive developmental plasticity. Molecular Ecology 20, 1347-1363.
497 Ben-Tabou de-Leon, S., Su, Y.H., Lin, K.T., Li, E., Davidson, E.H., 2013. Gene
498 regulatory control in the sea urchin aboral ectoderm: spatial initiation, signaling inputs,
499 and cell fate lockdown. Dev Biol 374, 245-254.
500 Breitburg, D., Levin, L.A., Oschlies, A., Gregoire, M., Chavez, F.P., Conley, D.J.,
501 Garcon, V., Gilbert, D., Gutierrez, D., Isensee, K., Jacinto, G.S., Limburg, K.E., Montes,
502 I., Naqvi, S.W.A., Pitcher, G.C., Rabalais, N.N., Roman, M.R., Rose, K.A., Seibel, B.A.,
503 Telszewski, M., Yasuhara, M., Zhang, J., 2018. Declining oxygen in the global ocean and
504 coastal waters. Science 359.
505 Breus, O., Dickmeis, T., 2020. Genetically encoded thiol redox-sensors in the zebrafish
506 model: lessons for embryonic development and regeneration. Biol Chem.
507 Carmeliet, P., 2005. VEGF as a key mediator of angiogenesis in cancer. Oncology 69
508 Suppl 3, 4-10.
509 Chang, W.L., Chang, Y.C., Lin, K.T., Li, H.R., Pai, C.Y., Chen, J.H., Su, Y.H., 2017.
510 Asymmetric distribution of hypoxia-inducible factor alpha regulates dorsoventral axis in
511 the early sea urchin embryo. Development 144, 2940-2950.
512 Chi, A.Y., Waypa, G.B., Mungai, P.T., Schumacker, P.T., 2010. Prolonged hypoxia
513 increases ROS signaling and RhoA activation in pulmonary artery smooth muscle and
514 endothelial cells. Antioxid Redox Signal 12, 603-610.
515 Coffman, J.A., Coluccio, A., Planchart, A., Robertson, A.J., 2009. Oral-aboral axis
516 specification in the sea urchin embryo III. Role of mitochondrial redox signaling via
517 H2O2. Dev Biol 330, 123-130.
518 Coffman, J.A., Davidson, E.H., 2001. Oral-aboral axis specification in the sea urchin
519 embryo. I. Axis entrainment by respiratory asymmetry. Dev Biol 230, 18-28.
520 Coffman, J.A., McCarthy, J.J., Dickey-Sims, C., Robertson, A.J., 2004. Oral–aboral axis
521 specification in the sea urchin embryo: II. Mitochondrial distribution and redox state
522 contribute to establishing polarity in Strongylocentrotus purpuratus. Dev Biol 273, 160-
523 171.
524 Coffman, J.A., Su, Y.H., 2019. Redox regulation of development and regeneration. Curr
525 Opin Genet Dev 57, 9-15.
526 Coffman, J.A., Wessels, A., DeSchiffart, C., Rydlizky, K., 2014. Oral-aboral axis
527 specification in the sea urchin embryo, IV: hypoxia radializes embryos by preventing the
528 initial spatialization of nodal activity. Dev Biol 386, 302-307.
529 Compernolle, V., Brusselmans, K., Franco, D., Moorman, A., Dewerchin, M., Collen, D.,
530 Carmeliet, P., 2003. Cardia bifida, defective heart development and abnormal neural crest
531 migration in embryos lacking hypoxia-inducible factor-1alpha. Cardiovasc Res 60, 569-
532 579.
533 Cordeiro, I.R., Tanaka, M., 2020. Environmental Oxygen is a Key Modulator of
534 Development and Evolution: From Molecules to Ecology: Oxygen-sensitive pathways
535 pattern the developing organism, linking genetic and environmental components during
536 the evolution of new traits. Bioessays 42, e2000025.
537 Czihak, G., 1963. Entwicklungsphysiologische untersuchungen an echiniden. Wilhelm
538 Roux'Archiv für Entwicklungsmechanik der Organismen 154, 272-292.

539   Desireddi, J.R., Farrow, K.N., Marks, J.D., Waypa, G.B., Schumacker, P.T., 2010.
540   Hypoxia increases ROS signaling and cytosolic Ca(2+) in pulmonary artery smooth
541   muscle cells of mouse lungs slices. Antioxid Redox Signal 12, 595-602.
542   Duboc, V., Lapraz, F., Besnardeau, L., Lepage, T., 2008. Lefty acts as an essential
543   modulator of Nodal activity during sea urchin oral-aboral axis formation. Dev Biol 320,
544   49-59.
545   Duboc, V., Lapraz, F., Saudemont, A., Bessodes, N., Mekpoh, F., Haillot, E., Quirin, M.,
546   Lepage, T., 2010. Nodal and BMP2/4 pattern the mesoderm and endoderm during
547   development of the sea urchin embryo. Development 137, 223-235.
548   Duboc, V., Rottinger, E., Besnardeau, L., Lepage, T., 2004. Nodal and BMP2/4 signaling
549   organizes the oral-aboral axis of the sea urchin embryo. Dev Cell 6, 397-410.
550   Duloquin, L., Lhomond, G., Gache, C., 2007. Localized VEGF signaling from ectoderm
551   to mesenchyme cells controls morphogenesis of the sea urchin embryo skeleton.
552   Development 134, 2293-2302.
553   Dunwoodie, S.L., 2009. The role of hypoxia in development of the Mammalian embryo.
554   Dev Cell 17, 755-773.
555   Dyer, L.A., Pi, X., Patterson, C., 2014. The role of BMPs in endothelial cell function and
556   dysfunction. Trends Endocrinol Metab 25, 472-480.
557   Foo, S.A., Koweek, D.A., Munari, M., Gambi, M.C., Byrne, M., Caldeira, K., 2020.
558   Responses of sea urchin larvae to field and laboratory acidification. Sci Total Environ
559   723, 138003.
560   Fuhrmann, D.C., Brune, B., 2017. Mitochondrial composition and function under the
561   control of hypoxia. Redox Biol 12, 208-215.
562   Garcia de Vinuesa, A., Abdelilah-Seyfried, S., Knaus, P., Zwijsen, A., Bailly, S., 2016.
563   BMP signaling in vascular biology and dysfunction. Cytokine Growth Factor Rev 27, 65-
564   79.
565   He, C., Chen, X., 2005. Transcription regulation of the vegf gene by the BMP/Smad
566   pathway in the angioblast of zebrafish embryos. Biochem Biophys Res Commun 329,
567   324-330.
568   Hueng, D.-Y., Lin, G.-J., Huang, S.-H., Liu, L.-W., Ju, D.-T., Chen, Y.-W., Sytwu, H.-
569   K., Chang, C., Huang, S.-M., Yeh, Y.-S., 2011. Inhibition of Nodal suppresses
570   angiogenesis and growth of human gliomas. Journal of neuro-oncology 104, 21-31.
571   Hughes, D.J., Alderdice, R., Cooney, C., Kühl, M., Pernice, M., Voolstra, C.R., Suggett,
572   D.J., 2020. Coral reef survival under accelerating ocean deoxygenation. Nature Climate
573   Change 10, 296-307.
574   Lapraz, F., Besnardeau, L., Lepage, T., 2009. Patterning of the Dorsal-Ventral Axis in
575   Echinoderms: Insights into the Evolution of the BMP-Chordin Signaling Network. PLOS
576   Biology 7, e1000248.
577   Lapraz, F., Röttinger, E., Duboc, V., Range, R., Duloquin, L., Walton, K., Wu, S.-Y.,
578   Bradham, C., Loza, M.A., Hibino, T., Wilson, K., Poustka, A., McClay, D., Angerer, L.,
579   Gache, C., Lepage, T., 2006. RTK and TGF-β signaling pathways genes in the sea urchin
580   genome. Dev Biol 300, 132-152.
581   Lee, S.L., Rouhi, P., Dahl Jensen, L., Zhang, D., Ji, H., Hauptmann, G., Ingham, P., Cao,
582   Y., 2009. Hypoxia-induced pathological angiogenesis mediates tumor cell dissemination,
583   invasion, and metastasis in a zebrafish tumor model. Proc Natl Acad Sci U S A 106,
584   19485-19490.

18

585 Lendahl, U., Lee, K.L., Yang, H., Poellinger, L., 2009. Generating specificity and
586 diversity in the transcriptional response to hypoxia. Nat Rev Genet 10, 821-832.
587 Li, E., Materna, S.C., Davidson, E.H., 2012. Direct and indirect control of oral ectoderm
588 regulatory gene expression by Nodal signaling in the sea urchin embryo. Dev Biol 369,
589 377-385.
590 Low, N.H.N., Micheli, F., 2018. Lethal and functional thresholds of hypoxia in two key
591 benthic grazers. Marine Ecology Progress Series 594, 165-173.
592 Luo, Y.J., Su, Y.H., 2012. Opposing nodal and BMP signals regulate left-right
593 asymmetry in the sea urchin larva. PLoS Biol 10, e1001402.
594 Mavropoulou A.M, V.V., Sofianos S., 2020. Dissolved oxygen variability in the
595 Mediterranean Sea. J Mar Syst 208, 103348.
596 Medini, H., Cohen, T., Mishmar, D., 2020. Mitochondria Are Fundamental for the
597 Emergence of Metazoans: On Metabolism, Genomic Regulation, and the Birth of
598 Complex Organisms. Annu Rev Genet 54, 151-166.
599 Morgulis, M., Gildor, T., Roopin, M., Sher, N., Malik, A., Lalzar, M., Dines, M., Ben-
600 Tabou de-Leon, S., Khalaily, L., Ben-Tabou de-Leon, S., 2019. Possible cooption of a
601 VEGF-driven tubulogenesis program for biomineralization in echinoderms. Proceedings
602 of the National Academy of Sciences 116, 12353.
603 Nam, J., Su, Y.H., Lee, P.Y., Robertson, A.J., Coffman, J.A., Davidson, E.H., 2007. Cis-
604 regulatory control of the nodal gene, initiator of the sea urchin oral ectoderm gene
605 network. Dev Biol 306, 860-869.
606 Oliveri, P., Tu, Q., Davidson, E.H., 2008. Global regulatory logic for specification of an
607 embryonic cell lineage. Proc Natl Acad Sci U S A 105, 5955-5962.
608 Pagès, G., Pouysségur, J., 2005. Transcriptional regulation of the Vascular Endothelial
609 Growth Factor gene–a concert of activating factors*. Cardiovascular Research 65, 564-
610 573.
611 Pearse, J.S., 2006. Ecological role of purple sea urchins. Science 314, 940-941.
612 Peter, I.S., Davidson, E.H., 2011. A gene regulatory network controlling the embryonic
613 specification of endoderm. Nature 474, 635-639.
614 Potente, M., Gerhardt, H., Carmeliet, P., 2011. Basic and therapeutic aspects of
615 angiogenesis. Cell 146, 873-887.
616 Quail, D.F., Taylor, M.J., Walsh, L.A., Dieters-Castator, D., Das, P., Jewer, M., Zhang,
617 G., Postovit, L.M., 2011. Low oxygen levels induce the expression of the embryonic
618 morphogen Nodal. Mol Biol Cell 22, 4809-4821.
619 Quail, D.F., Walsh, L.A., Zhang, G., Findlay, S.D., Moreno, J., Fung, L., Ablack, A.,
620 Lewis, J.D., Done, S.J., Hess, D.A., Postovit, L.-M., 2012. Embryonic Protein Nodal
621 Promotes Breast Cancer Vascularization. Cancer Research 72, 3851.
622 Range, R., Lapraz, F., Quirin, M., Marro, S., Besnardeau, L., Lepage, T., 2007. Cis-
623 regulatory analysis of nodal and maternal control of dorsal-ventral axis formation by
624 Univin, a TGF-beta related to Vg1. Development 134, 3649-3664.
625 Schmidtko, S., Stramma, L., Visbeck, M., 2017. Decline in global oceanic oxygen
626 content during the past five decades. Nature 542, 335-339.
627 Semenza, G.L., 2012. Hypoxia-inducible factors in physiology and medicine. Cell 148,
628 399-408.

629 Sethi, A.J., Wikramanayake, R.M., Angerer, R.C., Range, R.C., Angerer, L.M., 2012.
630 Sequential signaling crosstalk regulates endomesoderm segregation in sea urchin
631 embryos. Science 335, 590-593.
632 Smith, S.J., Rebeiz, M., Davidson, L., 2018. From pattern to process: studies at the
633 interface of gene regulatory networks, morphogenesis, and evolution. Current Opinion in
634 Genetics & Development 51, 103-110.
635 Suh, S.S., Hwang, J., Park, M., Park, S.Y., Ryu, T.K., Lee, S., Lee, T.K., 2014. Hypoxia-
636 modulated gene expression profiling in sea urchin (Strongylocentrotus nudus) immune
637 cells. Ecotoxicol Environ Saf 109, 63-69.
638 Sun, Z., Ettensohn, C.A., 2014. Signal-dependent regulation of the sea urchin
639 skeletogenic gene regulatory network. Gene Expression Patterns 16, 93-103.
640 Tafani, M., Sansone, L., Limana, F., Arcangeli, T., De Santis, E., Polese, M., Fini, M.,
641 Russo, M.A., 2016. The Interplay of Reactive Oxygen Species, Hypoxia, Inflammation,
642 and Sirtuins in Cancer Initiation and Progression. Oxid Med Cell Longev 2016, 3907147.
643 Tettamanti, G., Grimaldi, A., Valvassori, R., Rinaldi, L., de Eguileor, M., 2003. Vascular
644 endothelial growth factor is involved in neoangiogenesis in Hirudo medicinalis
645 (Annelida, Hirudinea). Cytokine 22, 168-179.
646 Tiozzo, S., Voskoboynik, A., Brown, F.D., De Tomaso, A.W., 2008. A conserved role of
647 the VEGF pathway in angiogenesis of an ectodermally-derived vasculature. Dev Biol
648 315, 243-255.
649 Ushio-Fukai, M., Nakamura, Y., 2008. Reactive oxygen species and angiogenesis:
650 NADPH oxidase as target for cancer therapy. Cancer Lett 266, 37-52.
651 Vaquer-Sunyer, R., Duarte, C.M., 2008. Thresholds of hypoxia for marine biodiversity.
652 Proc Natl Acad Sci U S A 105, 15452-15457.
653 Wiley, D.M., Kim, J.-D., Hao, J., Hong, C.C., Bautch, V.L., Jin, S.-W., 2011. Distinct
654 signalling pathways regulate sprouting angiogenesis from the dorsal aorta and the axial
655 vein. Nature Cell Biology 13, 686-692.
656 Yoshida, M.A., Shigeno, S., Tsuneki, K., Furuya, H., 2010. Squid vascular endothelial
657 growth factor receptor: a shared molecular signature in the convergent evolution of
658 closed circulatory systems. Evol Dev 12, 25-33.
659

660

661

662

663

664

665

Figures legends
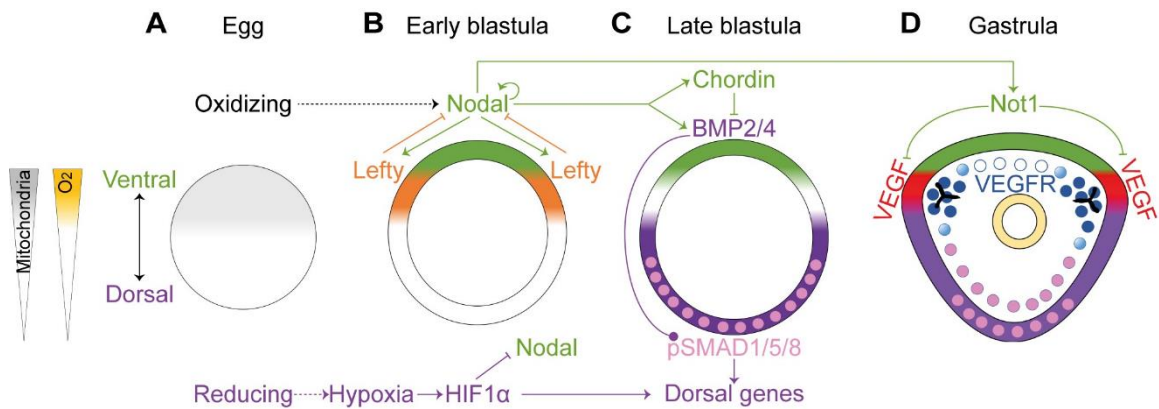
Figure 1 The regulation of DV axis formation downstream of redox and oxygen gradients in the sea urchin embryo. Diagrams showing sea urchin DV and skeletal patterning in developing sea urchin embryos in normal conditions based on (Chang et al., 2017; Coffman et al., 2009; Coffman and Davidson, 2001; Coffman et al., 2004; Coffman et al., 2014; Czihak, 1963; Duboc et al., 2004; Lapraz et al., 2009; Li et al., 2012). **(A)** The asymmetric distribution of mitochondria in the egg induces a redox gradient. **(B)** Regulatory interactions between *nodal*, *lefty* and HIF1α at the early blastula stage. **(C)** Nodal regulation of BMP signaling in the late blastula stage. **(D)** In the gastrula stage, Nodal activates the expression of Not1, that represses *VEGF* expression in the ventral ectoderm. Throughout the figure, the ventral side and Nodal expression domain are highlighted in green, the dorsal side and the domain of BMP activity are marked in purple. Nucleus that show pSMAD1/5/8 are highlighted in pink. *VEGF* expression is marked in red. *VEGFR* expression is marked in blue.

21

680
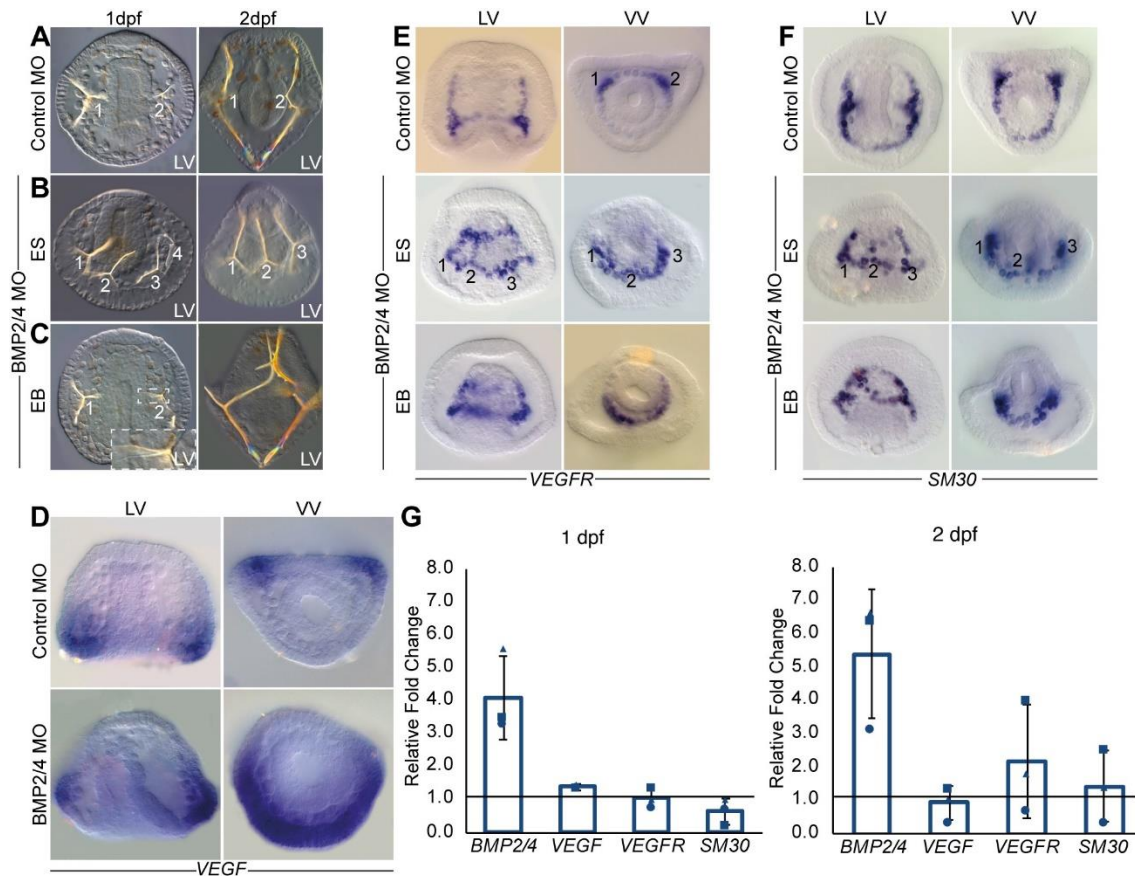
Figure 2 BMP2/4 controls skeletal patterning and VEGF expression. (A) Embryos injected with control MO show normal two spicules at 1dpf (left, 110/110 of scored embryos show this phenotype) and 2dpf (right, 56/56). **(B-C)** BMP2/4 MO injected embryos show either ectopic spicules indicated by numbers (ES, 89/169 1dpf, 120/135 2dpf) or ectopic spicule branching (EB, 39/169 at 1dpf, 15/135 at 2dpf). **(D)** VEGF expression is localized in two lateral patches in control embryo (top) and is strongly expanded in embryos injected with BMP2/4 MO at 1dpf (bottom). **(E-F)** VEGFR and SM30 expression in control embryo (top) and in BMP2/4 morphants (middle and bottom) at 1dpf. BMP2/4 MO leads to the expansion of the expression either into ectopic skeletal cell-clusters indicated by numbers (ES) or to continuous expansion (EB). LV, lateral view, VV, ventral view. Phenotypes are based on n≥3 independent biological replicates and spatial expression were observed in two independent biological replicates where n≥30 embryos were scored in each condition. **(G)** Ratio between gene expression in BMP2/4 MO compared to control MO embryos at 1dpf (left graph) and 2dpf (right graph). Bars show averages and markers indicate individual measurements of three independent biological replicates. Line marks ratio of 1 that indicates that the expression of the gene is unaffected by the perturbation. Error bars indicate standard deviation.
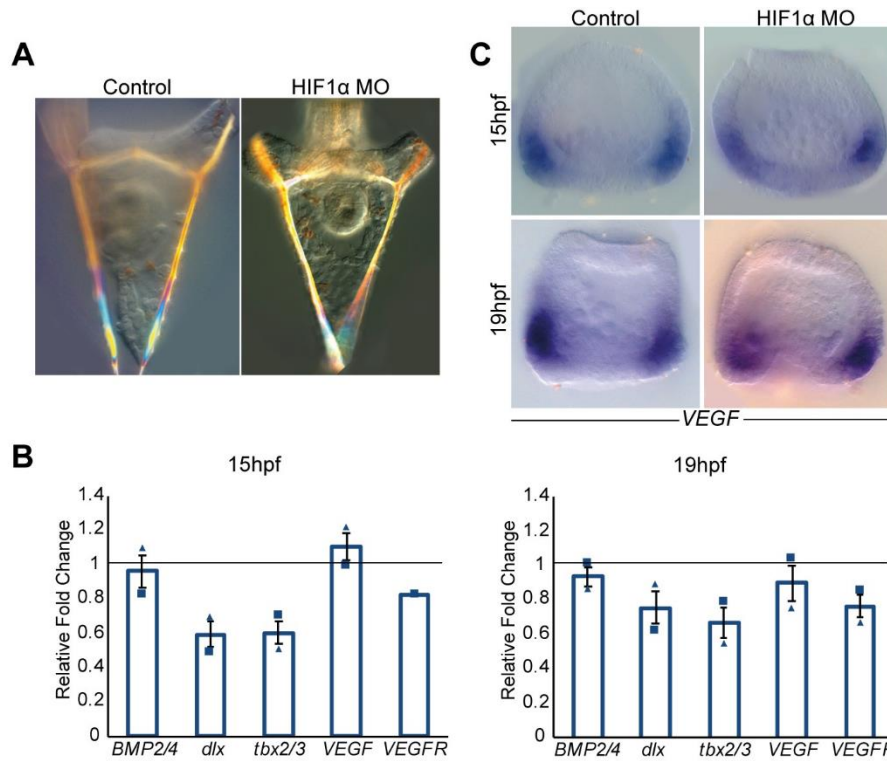
Figure 3 Sea urchin HIF1α does not affect skeletal patterning and VEGF expression. (A) Control (left) and HIF1α MO injected embryos (right) show comparable skeletal structure at 2dpf. **(B)** Ratio between gene expression in HIF1α MO compared to control MO embryos at 15hpf (left graph) and 19hpf (right graph). Bars show averages and markers indicate individual measurements of two independent biological replicates. Line marks ratio of 1 that indicates that the expression of the gene is unaffected by the perturbation. Error bars indicate standard deviation. **(C)** *VEGF* expression is similar in embryos injected with control MO (left) and HIF1α MO (right) at 15hpf (top) and 19hpf (bottom). Spatial expression were observed in two independent biological replicates where n≥30 embryos were scored in each condition.
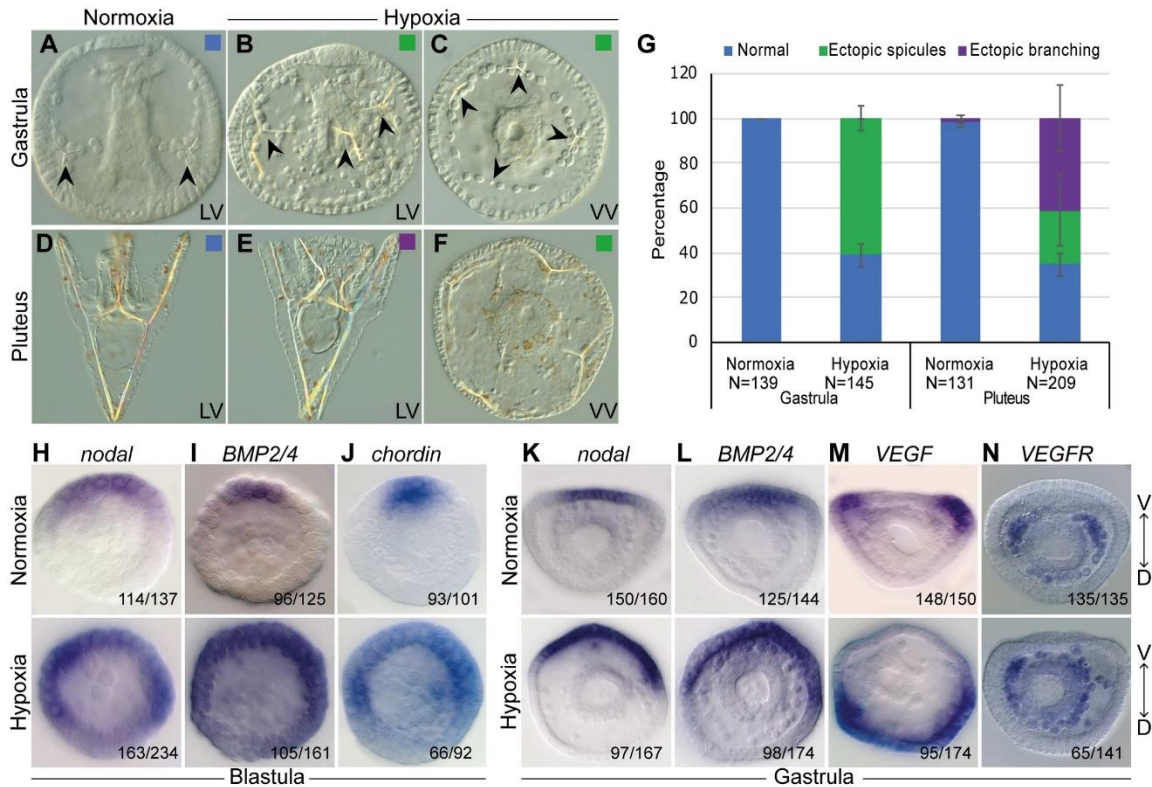
Figure 4 Growth in hypoxic condition leads to skeletal defects and perturbs the expression of DV and skeletal patterning genes. (A-C) Representative images of embryos at gastrula stage. **(A)** Embryo grown in normoxic conditions shows normal development of two spicules. **(B-C)** embryos grown in hypoxic condition show ectopic spicules, indicated by arrowheads. **(D-F)** Representative images of embryos at pluteus stage. **(D)** Embryo grown in normoxic conditions shows normal skeleton. **(E)** Embryo grown in hypoxic condition shows a normal DV axis and ectopic spicule branches. **(F)** Radialized embryo grown in hypoxic conditions that displays multiple ectopic spicules. LV, lateral view; VV, ventral view. **(G)** Quantification of skeletogenic phenotypes at gastrula stage and pluteus stage. Color code is indicated in the representative images. Error bars indicates standard deviation of three independent biological replicates. **(H-J)** Spatial expression of *nodal*, *BMP/4* and *chordin* genes in normoxic (top) and hypoxic embryos (bottom) at blastula stage. **(K-N)** Spatial expression of *nodal*, *BMP2/4*, *VEGF* and *VEGFR* genes in normoxic (top) and hypoxic embryos (bottom) at the gastrula stage. Embryos are presented in ventral view and the axis is labeled as V, ventral and D. Throughout H-N, the numbers at the bottom right indicate the number of embryos that show this expression pattern out of all embryos scored, based on three independent biological replicates.
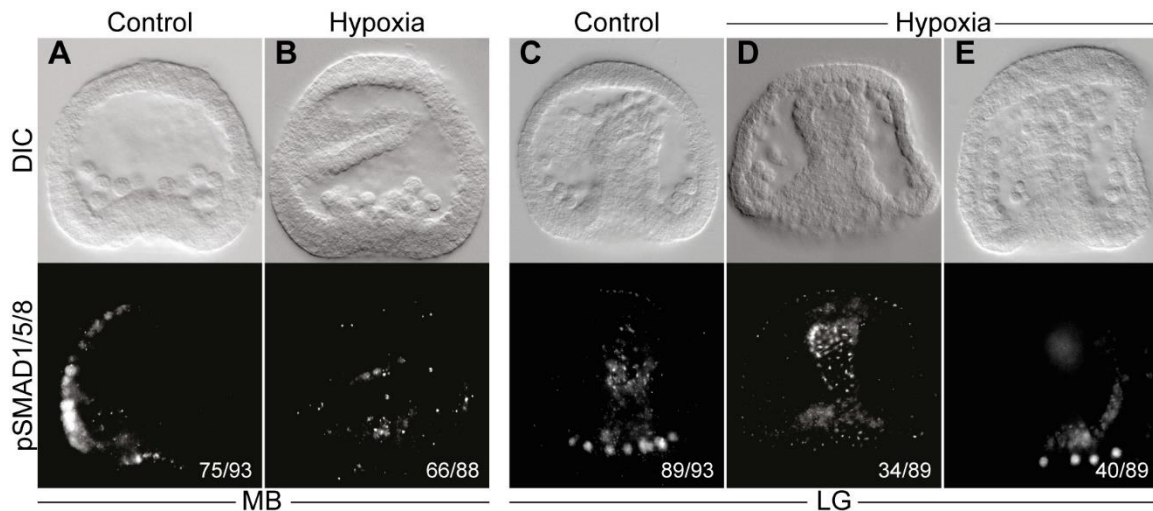
24

Figure 5 BMP activity is reduced in hypoxic conditions. (A-B) Nuclear pSMAD1/5/8 patterning in normoxic and hypoxic conditions at mesenchyme blastula (MB) stage. In normoxic conditions, pSMAD1/5/8 staining is detected in the dorsal ectoderm (A), while in hypoxic embryos the signal is completely abolished (B). **(C-E)** pSMAD1/5/8 staining in normoxic vs. hypoxic embryos at late gastrula (LG) stage. pSMAD1/5/8 is detected in the nuclei of the dorsal skeletogenic cells of normoxic embryos (C), while in hypoxic conditions the signal is either not detectable (D) or strongly reduced (E). DIC images of the embryos are presented in the upper row of each panel, and immunostaining of pSMAD1/5/8 of the embryos are presented in the lower row. All embryos are presented in lateral view (LV). The numbers shown on the bottom right of each figure indicate the number of embryos that show this expression pattern out of all embryos scored, based on three independent biological replicates.
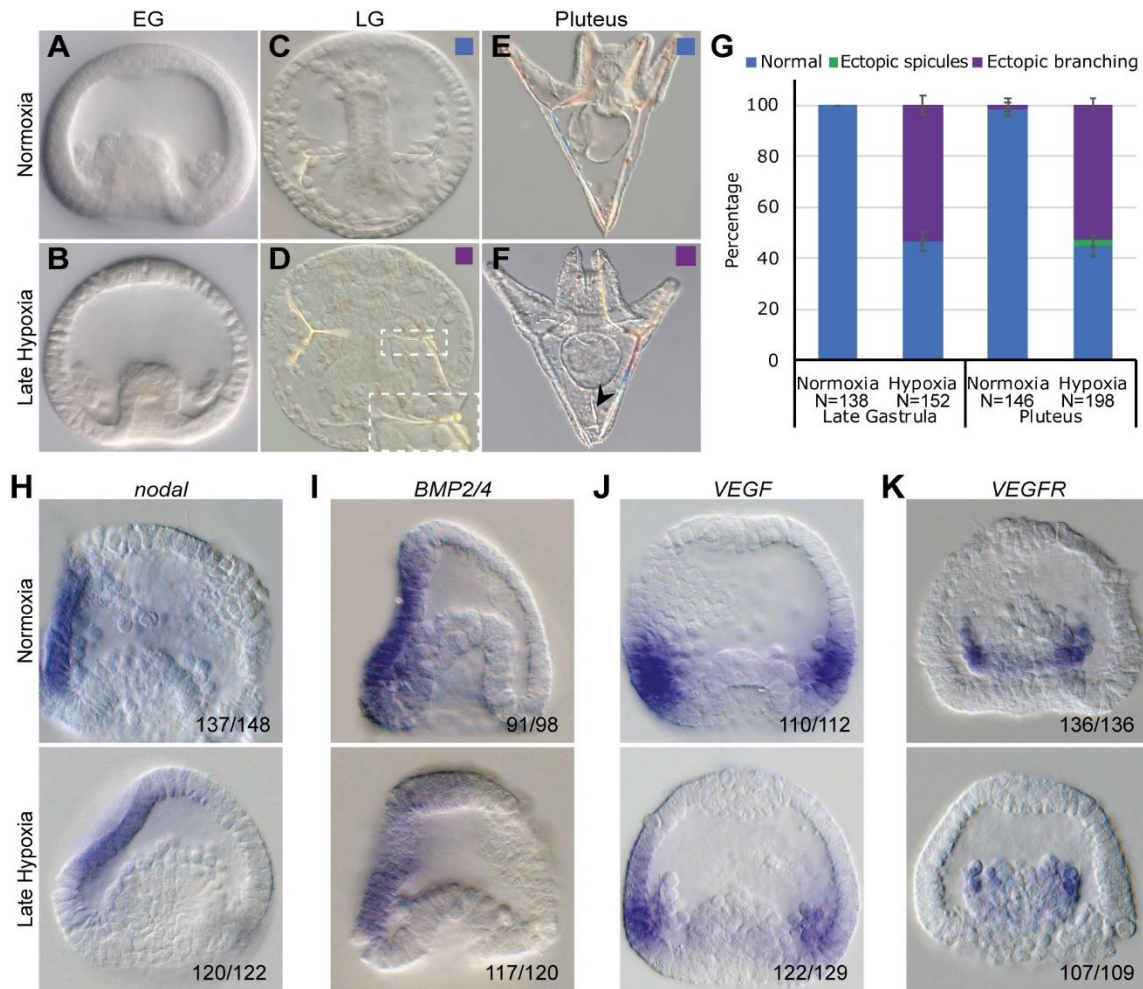
Figure 6 Late hypoxia affects skeletal structure but not skeletal patterning. **(A-F)** Representative images of live embryos, normoxic embryos are presented in the upper row, and equivalently staged hypoxic embryos are on the bottom. **(A-B)** Embryos at early gastrula stage show similar morphology in normoxia and hypoxia. **(C-D)** Hypoxic embryo at late gastrula stage shows two spicules with ectopic spicule branching (D) that are not observed in the normoxic embryo (C). Dashed white square is an enlarged image of the abnormal spicules. **(E-F)** Embryos at pluteus stage. Arrowhead in F, indicates an abnormal spicule growth in the hypoxic embryo. **(G)** Quantification of late hypoxia experiment over three biological replicates. Color code is indicated in the representative images. Error bars indicates standard deviation of three independent biological repeats. **(H-K)** WMISH results of *nodal*, *BMP2/4*, *VEGF* and *VEGFR* at early gastrula stage. Normoxic embryo is presented in the top and hypoxic embryo is in the bottom of each panel. On the bottom right of each figure we indicate the number of embryos that show this expression pattern out of all embryos scored, based on three independent biological replicates.
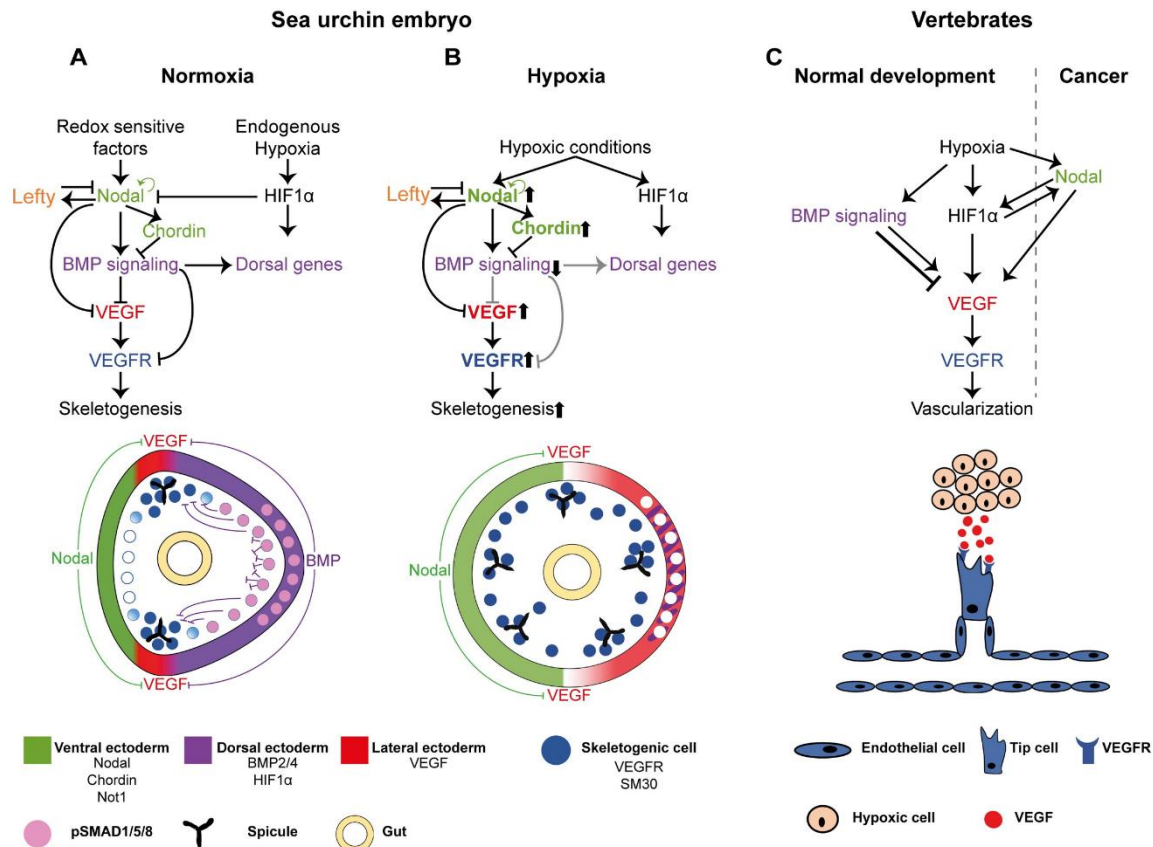
Figure 7 The interactions between the DV and skeletogenic GRNs, the response to early hypoxia and the similarities to the regulation of vertebrate's vascularization. (A-B) Diagrams showing our proposed model for skeletal patterning in normal conditions **(A)** and Hypoxic conditions **(B)**. Color codes are indicated in the bottom part of the figure. **(A)** The regulatory interactions between Nodal, BMP, HIF1α and VEGF signaling during normal development. BMP represses *VEGF*, *VEGFR* and *SM30* expression in the dorsal side and HIF1α does not regulate VEGF expression in the sea urchin embryo **(B)** The modification of the regulatory states in hypoxic conditions applied at early development, revealed in this work. Early hypoxia expands *nodal* expression and reduces BMP activity and the dorsal ectoderm. The reduction of BMP activity leads to an expansion of *VEGF*, VEGFR and *SM30* expression in the dorsal side and growth of ectopic skeletal centers. Ascending arrows near a gene name indicate enhanced activity, while descending arrows indicate reduced activity. Gray regulatory links indicate inactive connections under hypoxic conditions. **(C)** Diagram showing the relevant regulatory interactions during vertebrates' vascularization in normal development and in cancer, see text for explanations.